ISSN 0020-4412, Instruments and Experimental Techniques, 2008, Vol. 51, No. 3, pp. 428–433. © Pleiades Publishing, Ltd., 2008.
Original Russian Text © V.V. Zav'yalov, E.A. Zotova, E.Yu. Shamparov, 2008, published in Pribory i Tekhnika Eksperimenta, 2008, No. 3, pp. 109–114.

GENERAL EXPERIMENTAL TECHNIQUES

A Two-Channel Two-Frequency Low-Temperature Photodetector at Wavelengths of 119 and 220 μm of an H_2O Laser

V. V. Zav'yalov, E. A. Zotova, and E. Yu. Shamparov

Kapitza Institute for Physical Problems, Russian Academy of Sciences, ul. Kosygina 2, Moscow, 119334 Russia

Received September 27, 2007

Abstract—The design and characteristics of a compact device consisting of four cooled photodetectors of radiations at two frequencies (2.53 and 1.36 THz) are presented. The photodetectors are based on two pairs of Ge:Sb and *n*-type InSb single crystals and equipped with preamplifiers. The photodetector is intended for operating jointly with an H_2O laser, which operates in a mode of generation of orthogonally polarized waves, and can be used in interferometers with insufficiently stable lengths of optical paths, e.g., during investigation of plasma in high-power pulsed facilities. The photodetector is manufactured in the form of an insert into a commercial portable helium Dewar flask with a 12-mm-diameter neck.

PACS numbers: 52.70.-m, 07.57.Kp

DOI: 10.1134/S0020441208030196

INTRODUCTION

Two-frequency detectors of terahertz laser radiation can be used, e.g., during plasma investigations on high-power pulsed facilities, the operation of which is usually accompanied by mechanical vibrations of facilities during pulses. This circumstance substantially restricts the capabilities of laser interferometry of plasma, because vibrations cause uncontrollable variations in the length of the interferometer arms. Measurements are especially difficult to perform if the change in the optical-path length exceeds the wavelength of the probing radiation. Under such conditions, the accuracy of interferometric measurements can be improved considerably if a terahertz H_2O laser operating in a cw mode [1] serves as the radiation source. This laser's resonator is formed by a concave mirror and a thin metallic grid with a small mesh (30–60 μm) and square holes. If the grid is slightly stretched in the direction of one diagonal of squares, the effective lengths of the laser resonator become slightly different for the resonator's linearly polarized orthogonal modes. As was shown in [2], such a laser emits one pair—or simultaneously several pairs—of waves of different lengths. Each pair consists of orthogonally polarized waves frequency-shifted relative to each other, thereby simplifying performance of heterodyne-type measurements.

As an example, Fig. 1 shows one of possible scheme of the interferometer [2, 3] that was successfully used to measure the electron concentration in the cross section of a plasma filament in experiments by Kapitza [4]. This interferometer is analyzed in detail (with allowance for nonideal polarizer, the presence of harmonics in the signal, frequency beats, etc.) in [2]; here, we briefly describe this instrument.

Laser radiation at each of working wavelengths consists of two coaxial linearly polarized waves:

$$E_i^s \sim \sin(\omega_i t); \quad E_i^p \sim \sin(\omega_i t + \Omega_i t),$$

where ω_i is the fundamental (terahertz) radiation frequency, Ω_i is the frequency of beats (several tens of kilohertz) determined by the resonator anisotropy, and *s* and *p* are the radiation-polarization directions parallel and normal to the plane of Fig. 1. Tuning the length of the H_2O-laser resonator allows setting a mode of simultaneous lasing at two wavelengths $\lambda_{1,2}$ = 118.6 and 220 μm, which correspond to frequencies $\omega_{1,2}/2\pi$ of 2.53 and 1.36 THz.

Since the orthogonally polarized waves are coaxial, their paths from the laser to the interferometer and from the interferometer to the photodetectors are equal and even a large ($>> \lambda_i$) instability of the optical-path length does not affect their mutual phase difference. Only on the segment between polarizers G_3 and G_4 where the waves are separated according to their polarizations into measurement channel *2* and comparison channel *3*, they acquire phase difference Φ that includes both a contribution from the measured object (plasma) and a parasitic contribution from an unstable difference of the lengths of the interferometer arms. Knowledge of the frequency dependence of the plasma dispersion and allowance for the dispersion-free character of instability of the difference of the interferometer arms' lengths allows consideration of the effect of the instability source via calculations using the measurement data at different wavelengths.

Grid polarizer G_1 is designed for mixing the orthogonal polarizations. It is oriented at an angle of 45° with respect to the directions of the wave polarizations, and,

after waves pass through it, interference signal U forms at the photodetector:

$$U \sim \sqrt{\alpha}\cos(\Omega_i t + \Phi),$$

where α is the power transmission coefficient for the measurement channel.

Part of the radiation of both polarizations is branched into reference channel *1* by divider *S* and mixed with polarizer G_2.

Hence, two radiation fluxes propagate in the interferometer: the main flux consisting of two coaxial Gaussian laser-radiation beams at wavelengths of 118.6 and 220 μm, each of which carries information on the phase and amplitude of the wave passing through plasma, and the reference flux that allows continuous control of the amplitude and initial phase of beats of each of the aforementioned waves.

Because both the parameters of pulsed-discharge plasma and the spectrum of the device vibrations slightly change from pulse to pulse, to improve the measurement accuracy, it is necessary to simultaneously detect signals at both wavelengths in the interferometer.

Below, we describe the design and characteristics of the two-channel detector for simultaneous detection of laser radiation with beats of orthogonal polarizations at wavelengths of 118.6 and 220 μm for the interferometric scheme of plasma measurements.

DESIGN

Information on the measured object can be extracted from the ratio of amplitudes and the phase difference of the signals of the reference and measurement channels at each operating wavelength (118.6 and 220 μm) of the interferometer.

To attain a high sensitivity of radiation detection, we used semiconductor photoresistors cooled to $T = 4.2$ K. Crystals of germanium doped with antimony (Ge:Sb) and *n*-type indium antimonide (*n*-type InSb) in a magnetic field were used to detect radiations at wavelengths of 118.6 and 220 μm, respectively.

The reference and measurement channels have the same design, but each channel has an individual pair of detecting crystals. The wavelength-separated radiation detection in each channel is attained owing to the different selective characteristics of crystals.

Activation energy E_a of Sb impurities in Ge is 9.6 meV [5]. The impurity absorption is high at wavelengths shorter than

$$\lambda_r = hc/(E_a + k_B T),$$

a value equal to 125 μm for Ge:Sb at 4.2 K. For germanium with other shallow impurities, impurity-absorption edge λ_r lies at shorter wavelengths (118 μm for Ge:Al, 115 μm for Ge:B, etc.), and H_2O-laser radiation at $\lambda = 118.6$ μm is absorbed in them less efficiently. At the same time, radiation at 220 μm is virtually not absorbed in Ge:Sb because this wavelength is appreciably longer than that corresponding to the photoemission threshold.

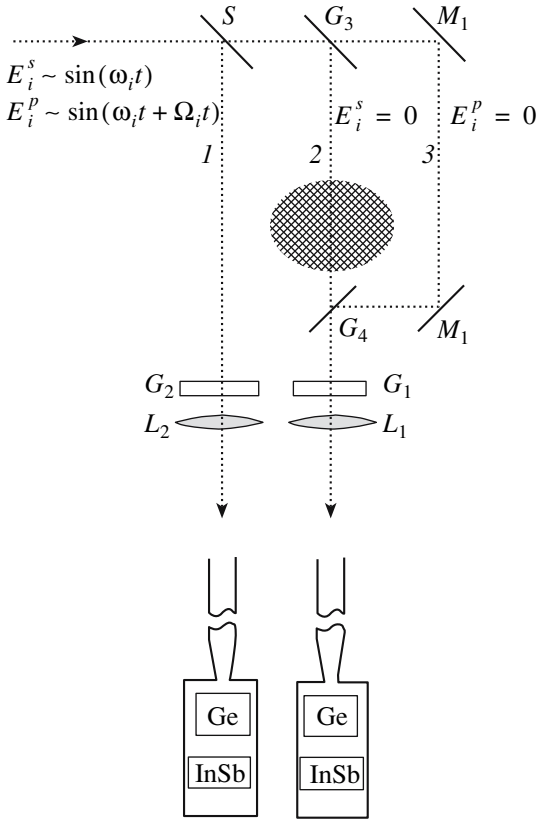

Fig. 1. One possible scheme for operation of the interferometer with beams from a diagnostic laser operating in the mode of generation of linear orthogonal polarizations: (*S*) beam splitter, (*G*) wire polarizer, (*M*) mirror, (Ge, InSb) photodetectors of the device for separate detection, (*L*) focusing lens, (*1*) reference channel, (*2*) measurement channel, and (*3*) comparison channel.

In InSb, radiation is detected within a narrow frequency band due to cyclotron-resonance absorption in a magnetic field. Figure 2 shows the dependences of the response of *n*-type InSb to radiation of the H_2O laser at (curve *2*) $\lambda = 118.6$ μm and (curve *1*) $\lambda = 220$ μm on the magnetic field. These curves were measured with the detector described in [6]. From these curves, we have found the value of magnetic field $B = 0.55$ T optimized for selective detection, at which *n*-type InSb is highly sensitive at a wavelength of 220 μm at a large ratio of the signals at 220 and 118.6 μm.

Ge:Sb and *n*-type InSb crystals have similar optical characteristics. Germanium has a refractive index of $n = 4.0$, and the penetration depth at $\lambda = 118.6$ μm is ~1 cm. Indium antimonide has a refractive index of $n = 4.1$, and the penetration depth at $\lambda = 220$ μm is 1.5 cm [6]. This circumstance allows simultaneous and efficient use of these crystals in a common optical system.

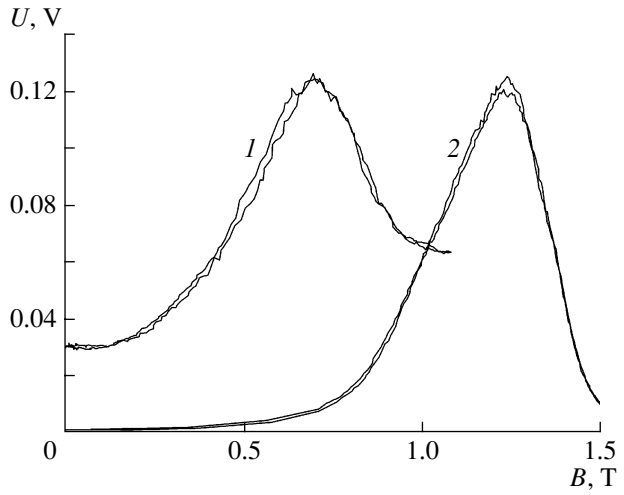

Fig. 2. Responses of the InSb detector to radiation at wavelengths of (*1*) 220 and (*2*) 118.6 μm vs. magnetic field.

Identical (symmetric) integrating chambers are used in each channel. Such a chamber—an almost closed cavity with high-reflectivity walls and a small hole for radiation injection—allows a considerable increase in the absorption owing to a large number of radiation passes through the detecting crystal. Each chamber has a 20-mm^2 cross section and a 0.8-mm^2-area hole for radiation injection. A 3-mm-thick *n*-type InSb single crystal and a 2-mm-thick Ge:Sb single crystal with a cross-sectional area of ~15 mm^2 are placed in each chamber. The first crystal positioned on the radiation path is Ge:Sb, which almost does not absorb radiation at $\lambda = 220$ μm. In this case, the amount of radiation at $\lambda = 118.6$ μm that reaches the *n*-type InSb crystal decreases, thereby additionally improving the detection selectivity.

The entire detector is designed in the form of an insert (Fig. 3) in a 10-liter portable helium Dewar flask produced in Russia (with a 12-mm inner diameter of the flask neck). The low-temperature unit (Fig. 4), which includes collecting cones *1*, integrating chambers *3* and *4*, magnetic system (b), and board *9* with preamplifiers, is immersed into the flask and cooled to $T = 4.2$ K. The cooled part is attached to the insert's top (see Fig. 3) with two 4-mm-diameter stainless steel tubes *2*. The tubes simultaneously serve as light guides through which radiation arrives at the detecting crystals. In addition, four 1-mm-diameter tubes, through which wires supplying voltages and outputting signals from the detecting crystals run, are connected to the low-temperature part. All tubes are encased in 11-mm-diameter outer tube *15* matched to the vacuum-tight gasket at the top of the portable Dewar flask. The bottom of the outer tube reaches only the top of the flask's helium chamber. The top of tube *15* is vacuum-tightly soldered to flange *14*, which is attached to the instrument's aluminum body *8*, inside which rechargeable batteries and electronic boards are placed and on the surface of which are connectors, control elements, and indicators.

Two light guides run through flange *14* and the instrument's case. On the case's upper surface, they are soldered into flange *13*, in which there are entrance windows *12* covered with black polyethylene. This material virtually does not transmit radiation at $\lambda < 20$ μm, thus reducing the undesirable illumination of detecting crystals. The detected radiation passes through the entrance windows and light guides and enters the low-temperature unit, where, by means of two cones *1* with polished surfaces (see Fig. 4), radiation is collected inside integrating chambers *3* and *4*. Owing to the cones, on the one hand, the entrance area increases (two entrance windows with a 10.3-mm^2 area each) and, on the other hand, the detector's angle of view decreases, thereby reducing the spurious side illumination and favoring measurements with narrowly directed radiation from the H_2O laser. The measured angle of view was ±10° (solid angle $\Omega = 0.1$ sr).

The *n*-type InSb crystal is placed in the magnetic field that is created by a system comprising permanent magnets (see Fig. 4b). The geometry of the magnetic system was chosen on the basis of the requirements of a compact and simple design. In addition, the field induction inside the *n*-type InSb crystal must be close to an optimal value (0.45–0.65 T); the field must be uniform to an acceptable degree at quite a significant spread in directions (±45°), which ensures more complete absorption of almost diffuse radiation inside the chamber. At the location of Ge:Sb crystals *2*, the field induction must be low (<0.1 T).

The pair of integrating chambers is assembled of two parts. Upper part *4* of the case of the integrating chambers is manufactured from soft magnetic steel and serves as an element of the magnetic circuit for creating the field applied to the InSb crystals and as a shield for Ge:Sb crystals. Bottom part *3* is made from copper and specifies the size of the magnetic gap in which both InSb crystals *5* are positioned. The cavities of both parts are divided by a copper partition, which is tightly fitted to the walls, into two integrating chambers. The magnetic field is created by a stack of four permanent magnets *7* (Alnico type with a residual induction of ~1 T) 1 mm thick each, which are tightly fitted and inserted into a groove in bottom part *3*. The top of the stack of magnets abuts against the partition between the integrating chambers. The reflecting nickel surface of the upper magnet is the lower wall of both integrating chambers. The bottom of the stack of magnets coincides with the edge of bottom part *3*.

Bottom part *3* is attached to upper part *4* with steel screw *6* through steel washer *8*. This screw and washer also serve as elements of the magnetic circuit. Board *9* with two cooled preamplifiers (one for each detecting Ge:Sb crystal) is soldered to a protrusion on the washer. An 11-mm-diameter thin-walled stainless steel tube (not shown in Fig. 4) is soldered coaxially to the bottom

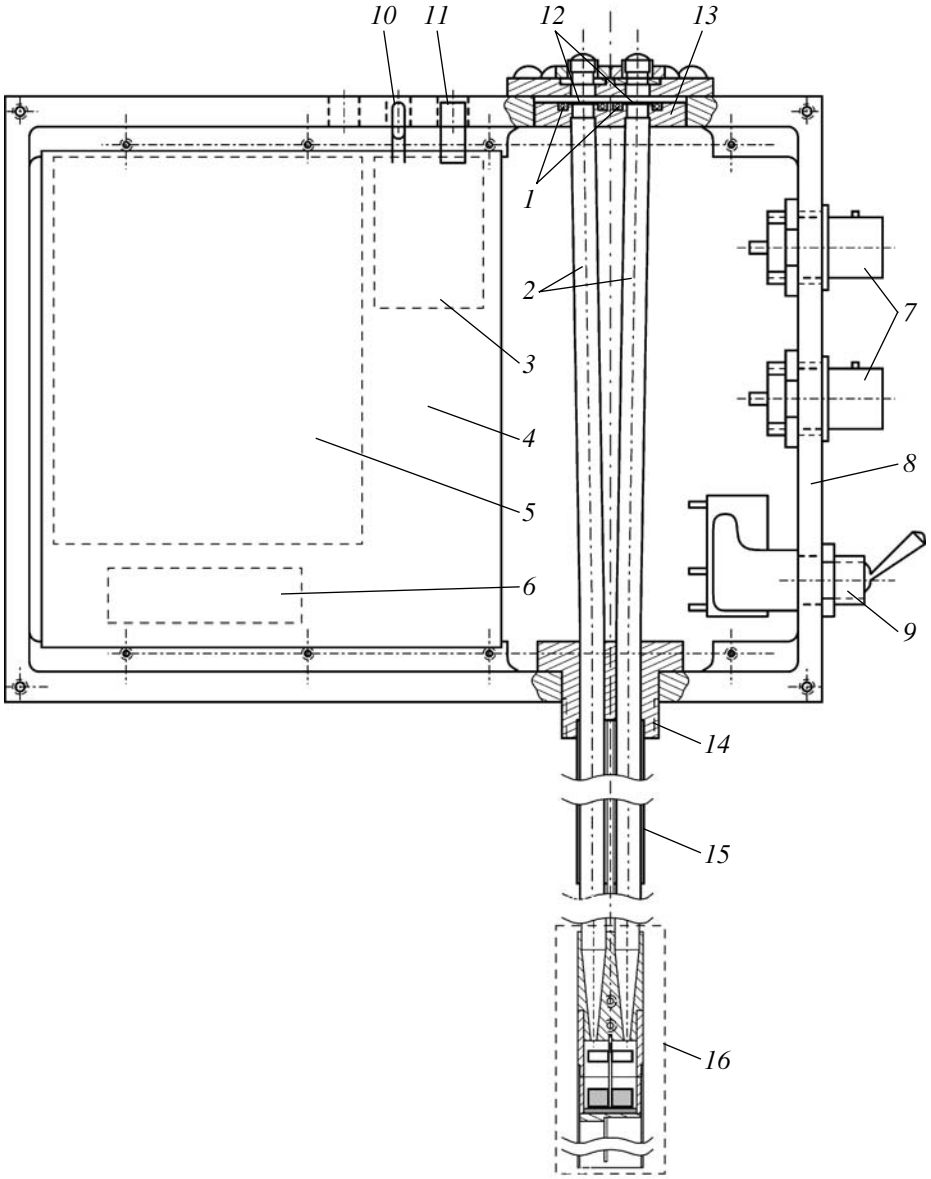

Fig. 3. Design of the insert: (*1*) vacuum seal (O-ring), (*2*) optical channels, (*3*) battery-charging unit, (*4*) board, (*5*) assembly of accumulator batteries, (*6*) unit for adjusting the bias voltage across crystals, (*7*) outputs, (*8*) case, (*9*) switch, (*10*) LED for indicating the charge of the batteries, (*11*) connector for charging the batteries, (*12*) entrance windows, (*13*) upper flange, (*14*) bottom flange, (*15*) 11-mm-diameter tube for the neck of the portable Dewar flask, and (*16*) low-temperature part.

of upper part *4*. Bottom part *3*, washer *8*, fastening screw *6*, and board *9* with the preamplifiers are tightly inserted into this tube, thereby ensuring precise arrangement and mechanical protection of the components against external effects.

The field induction of the permanent magnets was measured with a Ш1-8 magnetic-induction meter. The dimensions of the elements of the magnetic system and the magnetic-field induction were calculated with a computer.

The beat frequencies of the H_2O-laser radiation lie in the range 10–100 kHz; therefore, it is sufficient to take the value f_{up} = 200 kHz as the upper boundary frequency of the detector. The resistance of Ge:Sb crystals at the working point is ~300 kΩ, and capacitance C_l of the transmission line from the cooled to the high-temperature part of the detector is ~0.1 nF; these parameters would have resulted in an upper boundary frequency of measurements of $1/(2\pi R_g C_l)$ = 10 kHz. To extend the frequency range to 200 kHz, two cooled current preamplifiers placed at a minimum distance from the Ge:Sb crystals are included in the signal-processing circuit (Fig. 5). Each preamplifier is a source follower based on a КП350А insulated-gate silicon transistor

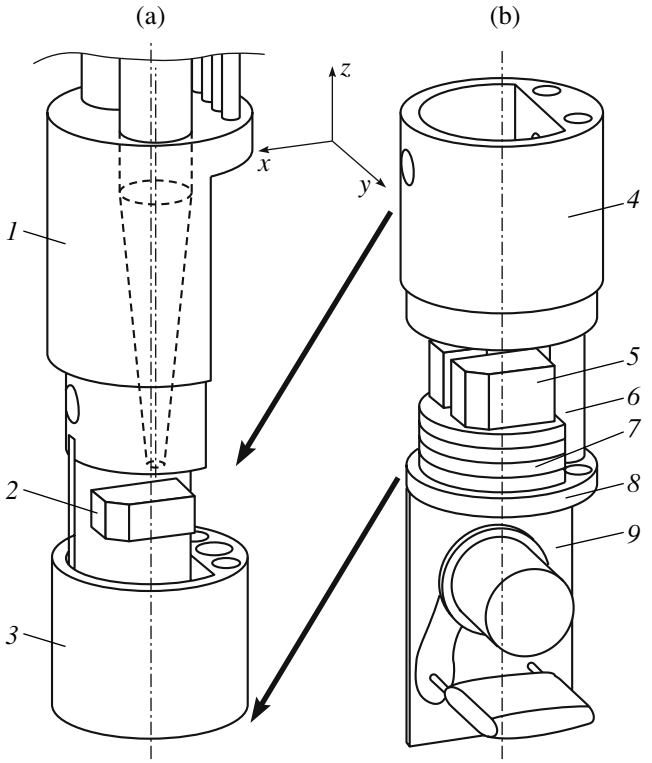

Fig. 4. Exploded view (a, b) of the low-temperature part of the insert, where (b) are the components of the magnetic circuit: (*1*) upper part with collecting cones; (*2*) Ge:Sb crystals; (*3*) bottom part of the integrating chamber with the partition to which detecting crystals are fixed; (*4*) upper part of the integrating chamber and the upper pole of the magnetic circuit; (*5*) InSb crystals; (*6*) fastening screw–back magnetic circuit; (*7*) stack of four permanent magnets; (*8*) washer for fastening parts, an element of the magnetic circuit; and (*9*) board with preamplifiers.

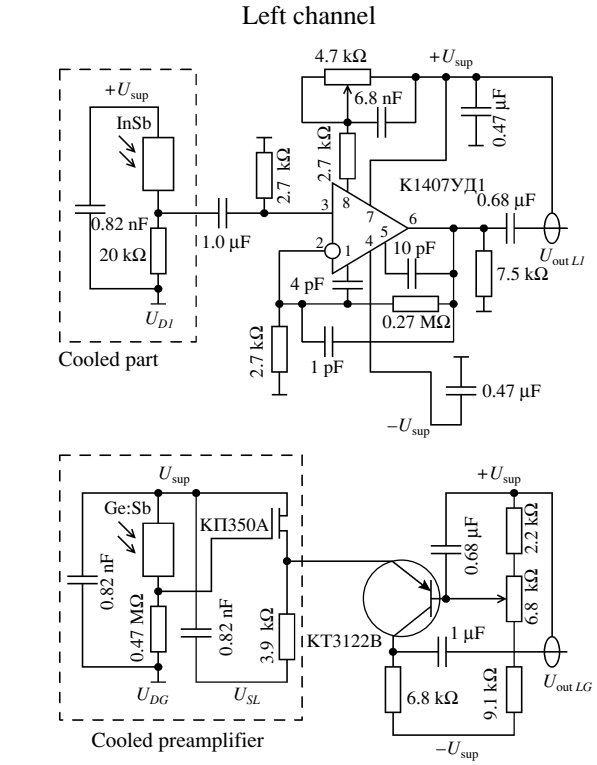

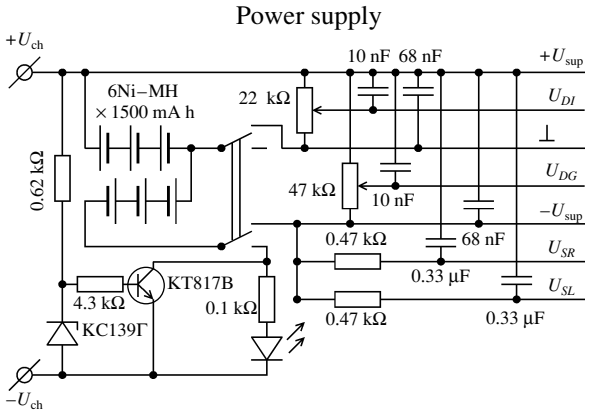

Fig. 5. Circuit diagram of the device.

that retains the working capacity in liquid helium. The follower reduces the output impedance of the cooled section of the circuit to ~1 kΩ, thus allowing transmission of signals without losses from the Ge:Sb crystals to the amplifiers having room temperature. As the latter amplifiers, we used transistor stages assembled according to the common-base circuit having a wide dynamic range of output voltages (±2 V). The gain of signals from the Ge:Sb detector is 10.

The resistance of detecting *n*-type InSb crystals at the working point is low (~10 kΩ), and it is unnecessary to use cooled preamplifiers. Signals are amplified by an rf amplifier based on a КР1407УД1 microcircuit. A negative feedback that specifies a voltage gain of 40 is applied to each integrated circuit, which incorporates frequency-correction elements for linear amplification within the specified frequency range. In addition, zero-correction circuits that allow attainment of a maximum output signal of up to ±2.5 V in each channel have been assembled and adjusted.

To ensure the possibility of operating with a mechanical radiation chopper (at a frequency of ~200 Hz), the chosen lower boundary frequency of the amplifiers is f_l = 150 Hz.

CALIBRATION AND CHARACTERISTICS

The photodetectors with detecting InSb crystals were calibrated according to the technique described in [6]. Equilibrium thermal radiation at room temperature, the response to which was measured with a mechanical mirror radiation chopper placed directly in front of the

entrance window of the PD, was used as the reference radiation. In this case, the illumination power irradiating the *n*-type InSb crystal is

$$W_b = \frac{k_B T_r A \Omega}{2\pi\lambda^2}\Delta\omega \approx 7.5 \times 10^{-8} \text{ W},$$

where $\Omega = 0.1$ Sr; $T_r = 293$ K is room temperature, $A = 10.3$ mm^2 is the area of the entrance window, $\lambda = 220$ μm, and $\Delta\omega = 5 \times 10^{12}$ rad/s is the radiation-absorption bandwidth in *n*-type InSb we measured earlier (see Fig. 2). Amplitude U_b of the response to room-temperature thermal radiation is 1.5 mV, and the volt–watt sensitivity of InSb PDs is

$$S_I = 2U_b/W_b = 40 \text{ V/mW}.$$

With allowance for the fact that the measured noise voltage was $U_n = 2$ mV, the detection ability was

$$D_I = S_I\sqrt{f_{up}}/U_n \approx 1.1 \times 10^{10}\sqrt{\text{Hz}}/\text{W}.$$

The obtained results are somewhat worse than the parameters of the InSb detector described in [6], but in view of its much more complex and not quite optimal geometry, they are quite acceptable. The volt–watt sensitivity of the PDs with the detecting Ge:Sb crystals to radiation at $\lambda = 118.6$ μm of the H_2O laser was determined from the comparison of their responses at this wavelength to the response of the *n*-type InSb PDs to radiation at $\lambda = 220$ μm. In this case, the ratio of the lasing powers of the H_2O laser at these two wavelengths was measured with a broadband pyroelectric PD.

These measurements were performed in the following manner. H_2O-laser radiation was split with a semitransparent mirror into two beams. One of them was directed to the pyroelectric PD and the other, to the input of a device with InSb and Ge:Sb PDs. The H_2O laser was tuned to generation of only 118.6-μm radiation, and responses of the Ge:Sb and pyroelectric PDs, U_G and U_{118}, were measured. The H_2O laser was then tuned to generation of only 220-μm radiation, and responses of the InSb and pyroelectric PDs, U_I and U_{220}, were measured. The volt–watt sensitivity of the Ge:Sb PDs was calculated from the formula

$$S_G = \frac{U_G}{U_I}\frac{U_{220}}{U_{118}}S_I \approx 400 \text{ V/mW}.$$

The noise voltage for the Ge:Sb PDs was 3 mV, and its detection ability was 7×10^{10} Hz$^{1/2}$/W.

The interference between the channels was as follows: crosstalk (from Ge:Sb to InSb or from InSb to Ge:Sb in the other channel), no more than 0.01 of the signal; and direct interference (from Ge:Sb to Ge:Sb or from InSb to InSb in the other channel), ~0.02 of the signal. The response of Ge:Sb to 220-μm radiation was found to be 35 times weaker than that to 118.6-μm radiation. The response of InSb to 118.6-μm radiation was found to be 20 times weaker than that to 220-μm radiation of the same power.

The selectivity of detection of radiation at $\lambda = 118.6$ and 220 μm in each channel can be substantially increased during narrow-band detection of signals from the PD output at beat frequencies different for each wavelength.

The consumption of liquid helium during continuous operation of the instrument is no higher than ~1 l/day.

REFERENCES

1. Zav'yalov, V.V. and Bogomolov, G.D., *Prib. Tekh. Eksp.*, 1982, no. 3, p. 174.
2. Zav'yalov, V.V., *Cand. Sci. (Phys-Math.) Dissertation*, Moscow: IFP AN SSSR, 1976.
3. Tishchenko, E.A., Zav'yalov, V.V., Zatsepin, V.G., and Lasarev, V.B., Abstracts of Papers, *Proc. XIII Int. Conf. Phenomena in Ionized Gases*, DDR, Berlin: 1977, p. 161.
4. Kapitza, P.L., *Zh. Eksp. Teor. Fiz.*, 1969, vol. 57, no. 6, p. 1801 [*Sov. Phys. JETP* (Engl. Transl.), vol. 57, no. 6, p. 973].
5. Seeger, K., *Semiconductor Physics*, Berlin: Springer, 1974. Translated under the title *Fizika poluprovodnikov*, Moscow: Mir, 1977.
6. Bogomolov, G.D., Zav'yalov, V.V., Zotova, E.A., and Shamparov, E.Yu., *Prib. Tekh. Eksp.*, 2002, no. 1, p. 87 [*Instrum. Exp. Tech.* (Engl. Transl.), no. 1, p. 78].